Towards optimization of polymer filament tensile test for material extrusion additive manufacturing process

Santiago Rodrigues[1], Seyed Miri[1], Richard G. Cole[2], Abraham Avalos Postigo[3], Menna A Saleh[4], Alexander Dondish[4], Garrett W. Melenka[4], Kazem Fayazbakhsh[1*]

[1]Department of Aerospace Engineering, Toronto Metropolitan University, Toronto, M5B 2K3, Canada

[2]National Research Council Canada, Aerospace Research Centre, Ottawa, K1A 0R6, Canada

[3]AON3D, Montreal, H2N 1P4, Canada

[4]Department of Mechanical Engineering, York University, Toronto, Canada

*Corresponding author: kazem@ryerson.ca; Tel: (+1) 416-979-5000 ext. 556414; fax: (+1) 416-979-5056; https://orcid.org/0000-0003-3963-8282

Abstract

Material extrusion (MEX) is a popular additive manufacturing (AM) method that can process a wide range of feedstock materials, most commonly in filament form. Currently, there is no standardized testing method for filament tensile properties, and researchers resort to 3D-printed dog-bone specimens, which necessarily include the effects of the printing process. In this study, the impact of the strain measurement device, knife-edge type, gage length, testing speed, and oven treatment on filament tensile properties was explored using an off-the-shelf fixture. It was observed that an extensometer with blunt knife edges, a filament gage length of 165 mm, and a 6.35 mm/min (0.25 in./min) testing speed could accurately evaluate the tensile properties of acrylonitrile butadiene styrene (ABS) filaments. In addition, an optimized raster path, 3D printing design, and process parameters were used to manufacture dog bone tensile specimens according to ASTM D638-22 from the same ABS filament spool. The tensile properties of the filaments were validated using the results of 3D-printed dog-bone specimens. Young's modulus, stress at yield, and stress at break for the optimum filament test set (2.20 GPa, 43.9 MPa, and 39.1 MPa) were very similar to those of the 3D-printed specimens (2.26 GPa, 44.9 MPa, and 37.3 MPa). The optimum filament tensile testing parameters determined in this study for ABS can be used for the initial test setup for other filament materials to provide baseline values that can serve as the foundation for AM process development.

Keywords:

Material extrusion (MEX), Fused filament fabrication (FFF), filament tensile testing, 3D-printed dog-bone specimens, ASTM D638 Type I, tensile properties.

Journal of Materials Research and Technology

https://doi.org/10.1016/j.jmrt.2023.05.088

1. Introduction

Additive manufacturing (AM), also known as 3D printing, shortens the design cycle by enabling rapid prototyping, increases design flexibility, and reduces material waste and lead time. The polymer material extrusion (MEX) process, also known as fused filament fabrication (FFF), is a simple and popular AM technique that can be applied to a wide range of feedstock materials. Many researchers have been working to understand the effects of MEX process parameters on the final mechanical properties of 3D-printed parts. However, an essential element of this work is missing: the reliable measurement of the properties of the material coming into the process to use as a baseline for assessing the effect of different process parameters. Furthermore, researchers have been developing new filament materials for the MEX process; however, reliable techniques to evaluate their mechanical properties are lacking.

Although a filament is a convenient form for the measurement of mechanical properties, there is currently no standardized testing technique for evaluating the tensile properties of filaments. Therefore, researchers and material suppliers have resorted to measuring the properties of 3D-printed tensile specimens, for example, dog-bone coupons per ASTM D638 or ISO 527, as an indication of filament material properties. Because the 3D-printing process and design parameters can significantly affect the mechanical properties, the specimens do not provide a reliable and robust means for assessing the filament material properties. Although 3D-printed tensile specimens have been extensively explored in the literature, the authors found only 23 research papers investigating the tensile properties of filaments, which are summarized in this section.

In the absence of a standardized filament tensile testing technique, researchers have explored several methods to evaluate the tensile properties of filaments. They can be categorized into three main groups based on the type of testing fixture: (1) use of testing machine grips, no fixture; (2) use of tabs; and (3) use of custom fixtures. Table 1 lists the studies that included filament tensile testing based on these three groups [1–23]. Because the focus of this study was on the testing procedure, information regarding the testing machine, load cell, strain measurement device, gage length, testing speed, filament diameter, and filament material is provided. Furthermore, some studies included the tensile testing of 3D-printed specimens and compared their tensile properties with the filament values.

Table 1. A detailed summary of filament tensile testing.

Testing fixture	#	Testing machine	Load cell (kN)	Strain measurement device	Gage length (mm)	Testing speed (mm/min)	Filament diameter (mm)[6]	Filament material	3D-printed specimen testing	Specimen type	Raster angle (°)
Grips	[1]	Zwick Z001	1	No	50	10	1.75	PLA[1], PP[2], PP- Glass-	No	Not applicable	Not applicable
	[2]	Zwick Z001	1	No	50	10	1.75	PP, PP- Glass	Yes	Shortened[15]	90
	[3]	Instron 33R4204	5	Extensometer	50	1	2.4-2.55 2.6-3.1	PP, PP-hemp/flax	Yes	ASTM D638 Type V	Concentric 0
	[4]	Zwick Z001	1	Not provided	50	10	1.75	PP, PP-cellulose	No	Not applicable	Not applicable
	[5]	Zwick	Not provided	High-speed camera	Not provided	5	1.75	PLA/PHA[3]-wood	Yes	ISO 527-1/2[16]	±45
	[6]	Zwick	10	High-speed camera	Not provided	5	1.75	PLA	Yes	ISO 527-1/2[16]	±45
	[7]	Zwick Z100	Not provided	Not provided	60	1	1.75	PLA PLA- G-CNF[4]	Yes	ASTM D638 Type IV	0/90 +45/-45
	[8]	TTM-01	25	Not provided	50	5	1.75	PLA, Bioparticle-PLA	No	Not applicable	Not applicable
	[9]	Zwick Z020	20	Extensometer	50	5	2.85	HDPE[5]- Glass microbaloons	Yes	ASTM D638 dog-bone[17]	±45
	[10]	Autograph AGS-X	5	Not provided	50	5	1.75	PA12[6], LAY-FOMM 60	Yes	ASTM D3039 straight-sided[16]	Hexagonal, linear
	[11]	Zwick	10	High-speed camera	Not provided	5	1.75	copolyester	Yes	ISO 527-1/2[16]	±45
	[12]	MTS	30	Not provided	Not provided	10	1.75	PA	No	Not applicable	Not applicable
	[13]	Imada MX2	Not provided	Not provided	Not provided	10	1.75	PC[7], PC-TiC[8]	Yes	ASSTM D638 Type V	±45
Grips with a cloth	[14]	LY-1066A	Not provided	Not provided	100	100	1.75	PLA virgin and recycled	No	Not applicable	Not applicable
	[15]	Instron 5567	Not provided	Not provided	50	Not provided	1.75	PA12, PA12-Mg[9]	Yes	ASTM D638 dog-bone[17]	+45
Grips with tabs	[16]	MTS Criterion 40	Not provided	Not provided	Not provided	0.06 (1/min)	2.85	PC	Yes[11]	ASTM D1708	0
	[17]	Instron 4468	5	No	Not provided	Not provided	0.7-0.98	ABS[10], ABS-HX8000	Yes	Straight-sided[15,16]	0,±45,90

	[18]	Instron 5969	Not provided	Not provided	Not provided	0.01 (1/min)	1.75	PA6-CF[11]	No	Not applicable	Not applicable
	[19]	Santam SMT-5	1	Not provided	60	1	1.75	PLA	No	Not applicable	Not applicable
Custom fixture	[20]	Testresources 312Q	10	Not provided	Not provided	5	1.75	PLA, PLA-GF[12]	Yes	ASTM D638 Type I	0
	[21]	Instron 4507	100	Not provided	Not provided	5	1.75	PETG[13], PETG-CF	Yes	ISO 527	+45
	[22]	UTS STM-50	2.22	Extensometer	Not provided	5	1.75	ABS	No	Not applicable	Not applicable
	[23]	Shimadzu AGS-X 50kN	1	No	200	5	1.75	PEI, PEI-CNT[14]	Yes	ASTM D638 Type IV	0, ±45
										ASTM D3039[16]	0

1. PolyLactic Acid (PLA), 2. Polypropylene (PP), 3. Poly Hydroxy Alkanoate (PHA), 4. Graphene-Carbon Nano Fiber (G-CNF), 5. High-Density Polyethylene (HDPE), 6. Polyamide 12 (PA12), 7. Polycarbonate (PC), 8. Titanium Carbide (TC), 9. Magnesium (Mg), 10. Acrylonitrile Butadiene Styrene (ABS), 11. Carbon Fiber (CF), 12. Glass Fiber (GF), 13. Poly Ethylene Terephthalate Glycol (PETG), 14. Poly Ether Imide (PEI) ULTEM1010-Carbon Nano Tubes (CNT), 15. No information regarding the testing standard for 3D-printed tensile specimen, 16. The specimen dimensions did not follow a standard type, 17. The specimen type was not provided.

Most studies on filament tensile properties used testing machine grips to introduce a load into the specimens [1-15] and observed significant stress concentration in the filaments near the grips. The use of tabs [16-19] reduced the stress concentration; however, it is known that tabs create a thickness discontinuity in a specimen and might result in premature failure. Another issue with placing a filament on testing machine grips, with or without a cloth or tab, is the unreliability of the elastic modulus measurements. It is challenging to make the filament completely straight at the beginning of the loading, and a slight filament curvature can result in high variability in the modulus calculations [2]. Several researchers have designed or used specialized fixtures [20-23] for filament tensile tests to ensure a pure and uniform load introduction to the specimens. Typically, these fixtures allow the winding of filaments around a bollard (a cylindrical load-introduction device), which simplifies the straightening of the filament at the beginning of the test.

Several studies, as shown in Table 1, did not use a strain measurement device during testing. The crosshead movement does not provide accurate elongation values before necking; therefore, it cannot be used for Young's modulus measurements. In addition, different gage lengths and testing speeds were used across the studies listed in Table 1, and their impact on the measurement of tensile properties was not explored. Almost none of the research articles described the filament failure location, that is, within the gage, apart from three studies [11, 14, 22]. Furthermore, 15 of the 23 studies compared the tensile properties of 3D-printed specimens to those of filaments and found lower values for 3D-printed coupons. Most studies used a rectilinear infill pattern with ±45 deg rasters, which does not provide tensile properties along the rasters in the gage section; therefore, they are inappropriate for comparison with filament values. Even the three studies that used 0° rasters in the gage section of dog-bone tensile specimens encountered major challenges in the transition area of the coupons, for example, large voids, resulting in unacceptable failure modes. Challenges with tensile testing of 3D-printed specimens were observed by many researchers and were summarized by Sola et al. [24].

Therefore, there is a limited amount of research studies on filament tensile testing, most of which encountered challenges such as filament stress concentration during testing and high variability in modulus measurements. In addition, they were not successful in validating filament tensile properties using 3D-printed dog-bone specimens.

This study focused on the filament tensile test procedure itself and explored the impact of several testing parameters on the successful measurement of the filament tensile properties. In addition, an optimized raster path was developed for 3D-printed dog-bone tensile specimens with 0° rasters in the gage section with minimum defects. The goal of this study was to develop an optimized test method for measuring the tensile properties of polymer filaments. Standardizing this method would benefit the additive manufacturing community by allowing the comparison of test results among research laboratories. Furthermore, material suppliers can provide datasheets

with filament tensile properties, which can be used for quality control checks during material purchases.

In this study, an off-the-shelf testing fixture, filament material, and oven-treatment process are described in Section 2. The test plan is then presented, which explores the impact of the following parameters on the filament tensile properties: the use of an extensometer with different knife edges, gage length, testing speed, and oven-treatment process. This is followed by a discussion of the raster optimization and 3D printing of dog-bone tensile specimens that are required to provide confidence in the filament tensile testing results. The testing procedure for the 3D-printed dog-bone specimens is also described. Section 3 summarizes the results of the filament and dog-bone tensile tests, followed by conclusions and directions for future research.

2. Methodology

2.1. Filament tensile testing

2.1.1. Fixture

As mentioned in the introduction, several researchers have used custom fixtures [20-23] for filament tensile testing. Rahimizadeh et al. [20] used a set of thimbles to fix the filaments in a testing machine. Ferreira et al. [21] designed a grip consisting of a clamping mechanism to fix the filament and bollard, where the filament was wrapped three times. They noted the difficulty of winding the filament around the bollard, particularly for less ductile filaments. Although the bollard diameter was not provided in their study, an image of the fixture indicated a bollard with a small diameter, which may have been the reason for the difficulties encountered. In a previous study [22], the authors designed a hook-shaped fixture with a diameter of 80 mm and 3D printed it from PLA. Although the filament installation and failure modes were robust, the clamping mechanism for the free ends of the filament was not always successful in preventing slippage. Yıldız et al. [23] used an off-the-shelf fixture comprising a bollard with a diameter of 150 mm and a vise.

From a literature review, it was observed that a set of fixtures consisting of a larger bollard diameter and a vise, where the filament is wound around the bollard and its free end is fixed, is a robust method for load introduction during filament tensile testing. The bollard diameter should be sufficiently large to prevent breakage of the filament during winding. The difference in extension between the inside and outside of the wound filament results in a strain that should be lower than that at the break. The minimum bollard diameter for preventing filament breakage can be calculated as follows (Eq. 1):

$$D_{fixture} = \frac{2 \times D_{filament}}{\varepsilon_b} \quad (1)$$

where $D_{fixture}$, $D_{filament}$, and ε_b are the minimum bollard diameter of the fixture, the diameter of the filament cross section, and the strain at break of the material, respectively. Although a large bollard

diameter is desirable to prevent filament breakage in the fixture, it reduces the available maximum head displacement of the testing machine and increases the required sample length.

In this study, a set of off-the-shelf fixtures and a high-capacity wire or rope grip G1092 (Mark-10 Corporation, Copiague, USA) were used, one for each end of the test specimen [25]. The 3D model files and dimensions of the fixture are available online [25] and provided in the data repository of this study. The bollard part of the fixture has a diameter of 92.9 mm; therefore, for a filament of 1.75 mm diameter, it can be used for testing materials with a strain at break of at least 3.77% (Eq. 1). Figure 1a shows the fixture, and Figure 1b shows a side view of the dimensions.

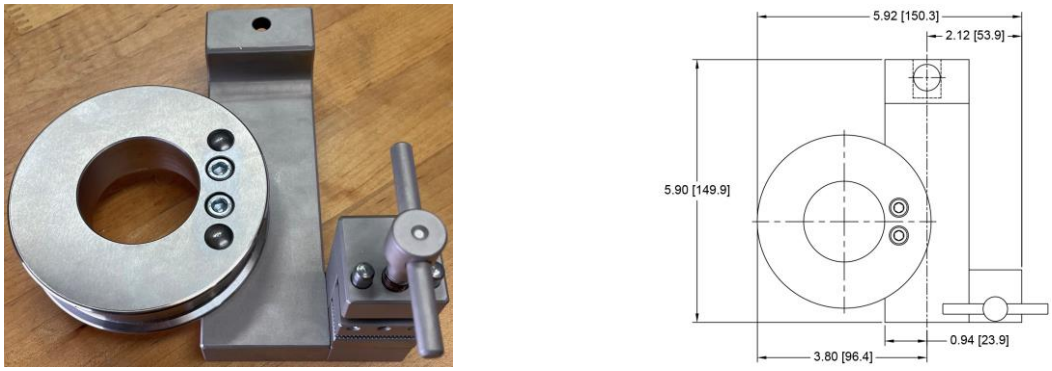

(a) **(b)**

Figure 1. G1092 fixture: (a) the fixture; and (b) dimensions in inches. [mm] [25].

2.1.2. Filament material and oven-treatment

An ABS Prime filament (AON3D, Montreal, Canada) with no pigmentation and a 1.75 mm nominal diameter was used for filament tensile testing and 3D printing dog-bone tensile specimens. A single filament spool was used in this study to minimize any variability caused by the materials (batch #CX09-0100-18-5LB, L000021J1121, S090100103001).

During filament manufacturing, the screw extrusion process, cooling, and winding procedures can result in preferential molecular alignment of the filament along its length. Rodriguez et al. [26] investigated ABS for the MEX process and observed that the degree of molecular orientation significantly affected the mechanical properties of thermoplastic polymers. They suggested filament oven treatment for several hours at a temperature 10°C above its glass transition temperature (T_g) to minimize this effect and allow the polymer molecules to relax to a more random orientation. Therefore, tensile testing of both the nontreated (as-received) and oven-treated filaments is of interest in this study.

Approximately 28 m of the ABS filament was rewound from plastic to a metallic spool and left loosely to ensure that the filament was free to shrink in length during the oven treatment. The filament was not cut into pieces to reduce waste and save material for the filament tensile testing, and an oven-treatment procedure at 111 °C ±0.1 °C, for a duration of 385 min, in an air-recirculated

oven was completed. At the end of the process, the filament slumped on the spool, was lightly stuck to itself, and was moderately wavy. Figure 2a shows the filament before oven-treatment; Figure 2b shows the spool inside the oven; and Figure 2c shows the spool at the end of the process.

(a) **(b)** **(c)**

Figure 2. Oven-treatment process: (a) non-treated filament; (b) the oven; and (c) oven-treated filament.

The oven-treatment process parameters (dwell temperature and time) followed those of the authors' previous study [22]. Furthermore, before the oven treatment of the spool, a piece approximately 85.5 cm long was cut and laid loose on the shelf in the oven. After 405 min at 111 °C, its length was reduced by 14.1% and its diameter was increased by 7.2%. These values agree with [22], where changes of -17% and +9% were observed for the filament length and diameter, respectively, for the same material (different lot).

2.1.3. Filament tensile testing procedure

As mentioned in the introduction, because there is no standardized testing for filament tensile properties, researchers have used crosshead movement for strain measurement, and the gage length and testing speed have varied across studies. In this study, first, using non-treated filaments, the impact of the strain measurement device, knife edge type, gage length, and testing speed was investigated (experiments A to H in Table 2). Then, experiment I explored the impact of oven-treatment on the filament's tensile properties. At least eight samples were tested in each experimental set.

Table 2. Filament tensile test plan.

Experiment ID	Strain measurement device	Knife edge type	Gage length, mm	Testing speed, mm/min (in./min)
A	No extensometer	N/A	165	6.35 (0.25)
B	Extensometer	Blunt		
C	Extensometer	Standard		
D	Extensometer	Blunt	250	9.65 (0.38)
E	Extensometer	Blunt	165	3.30 (0.13)
F				12.7 (0.5)

G				25.4 (1.0)
H				63.5 (2.5)
I[1]	Extensometer	Blunt	165	6.35 (0.25)

[1] Filaments were tested after oven-treatment. All other experiments were performed on non-treated filament.

It was realized that an optical extensometer creates minimal disturbance to the filament specimen; however, it presents challenges in measuring the strain considering the small filament diameter. A clip-on extensometer is available and is simple to implement. Preliminary experiments showed that the extensometer did not result in premature failure of the filament when blunt knife edges were used. The specimen gage length is defined as the straight section of the filament between the two bollards. It was initially decided to relate this to the specimen dimensions in ASTM D638-22, in which the grip-to-grip distances for the Type I and II specimens were 115 and 135 mm, respectively. After a review, it was observed that a filament gage length of at least 165 mm was required for proper extensometer placement. In accordance with the ASTM D638 standard, a test speed of 5 mm/min (0.2 in./min) ±25% is the lowest value for rigid and semirigid materials for Type I and II specimens. In this study, the speed increased proportionally because the filament length under tensile loading (165 mm) was longer than the grip-to-grip distance for the Type I specimens in ASTM D638 (115 mm). It was considered more important to match the strain rate inherent in the ASTM D638 standard rather than the absolute test rate.

As a result of the aforementioned considerations, an extensometer with blunt knife edges, a 165 mm gage length, and 6.35 mm/min (0.25 in./min) testing speed were chosen as the baseline parameters for filament tensile testing.

As listed in Table 2, experiments A, B, and C explored testing with no extensometer, an extensometer with blunt (rounded) knife edges, and an extensometer with standard (sharper) knife edges [27]. The gage length was explored in experiment D, where a 250 mm gage length (a 50% increase) was considered. A gage length greater than 250 mm was not possible for testing, considering the machine head displacement limit. As previously mentioned, 165 mm was the shortest length. In general, polymers are strain rate sensitive; therefore, for this larger gage length (compared to the baseline, 165 mm), the testing speed was proportionally increased from 6.35 mm/min (0.25 in./min) to 9.65 mm/min (0.38 in./min). For experiments E, F, G, and H, testing speeds of half, two, four, and ten times the baseline speed were investigated. While all previous experiments were performed on non-treated filaments, experiment I tested oven-treated filaments to explore the impact of this post-processing procedure on the tensile properties.

Two fixtures were installed on a UTS STM-50 testing machine (United Testing Systems, Concord, Canada) with a 2.22 kN (500 lbf) load cell. A 3542-025M-050-ST extensometer (Epsilon Technology, Jackson, USA) with a gage length of 25 mm and an elongation limit of 50% was used for the strain measurements. Standard (Part No. 350210-01) and rounded (Part No. 350210-BLUNT) extensometer knife edges were obtained from Epsilon Technology. Before testing, the

filament diameter was measured using a 3732XFL-1 digital micrometer (Starrett, Athol, USA) at five different points, and the average value was used for the calculations. Figure 3 shows the test setup, filament gage length, and extensometer placement using two elastic bands. The filament was wound only once around each bollard for all tests to minimize material usage.

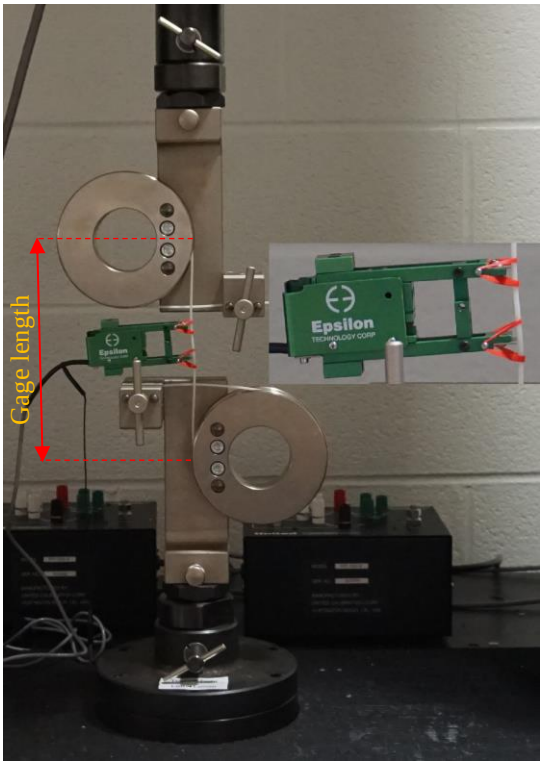

Figure 3. Filament tensile testing set-up.

The filaments were cut to the required length (approximately 90 cm for a gage length of 165 mm) on the testing day. Before testing, filaments were dehydrated at 60 ºC for one hour and placed inside a plastic bag with two 4A molecular sieve desiccant packages (Wisesorbent Technology LLC, Marlton, USA). Because the filaments were cut to length and placed inside the dehydrator, it was expected that one hour of dehydration would be sufficient. The laboratory environment was monitored using a HOBO MX1101 temperature and humidity logger (Onset, Bourne, USA). During testing, temperature and humidity were in the ranges of 24 to 25 °C and 17% to 37% relative humidity (RH), respectively.

2.2. Tensile testing of 3D-printed specimens

2.2.1 Optimization of raster path

As mentioned in the introduction, 15 of the 23 studies reviewed on filament tensile properties included testing of 3D-printed specimens. However, only three studies used 0° rasters in the specimen gage section, and all reported large voids in the transition area of the dog-bone tensile specimens [3, 20, 23]. These voids result in breakage outside the narrow cross-sectional test

section, which is an unacceptable failure mode according to ASTM D638. Although there have been studies on modifying specimen type and geometry of tensile specimens to achieve acceptable failure modes [28-32], the work reported here focused on the optimization of the raster path to manufacture dog-bone tensile specimens with dimensions and tolerances that do not deviate from the ASTM D638 standard.

The ASTM D638 Type I specimen was selected because it is the preferred sample with a material thickness of less than 7 mm. The raster path was defined as several concentric shells (outline perimeters) with ± 45° infill in the grip areas. All the extrudates in the gage section were along the specimen length (with a 0° orientation). To minimize the voids in the transition areas from the grips to the narrow section, the infill rasters were printed with an extra width of 22% (with respect to the outlines) and an outline overlap of 7%. Figure 4 shows the optimized raster path used in the 3D printing of dog-bone tensile specimens. A preliminary study on raster path optimization is included in the data repository of this study. Note that only Type I specimens were explored in this study, and the authors are currently considering a comparison between Type I and Type II specimens in future studies.

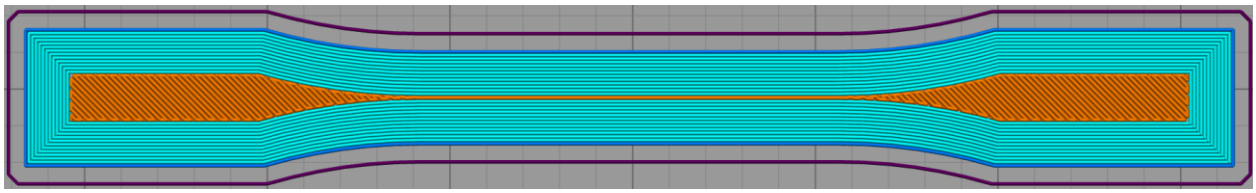

Figure 4. Optimized raster path of ASTM D638 Type I specimen for acceptable failure mode.

2.2.2 Specimen manufacturing

Many manufacturing and design parameters affect the mechanical performance of the MEX 3D-printed specimens. In addition to the raster path, these include the machine tolerance, build orientation, feedstock material, filament diameter, nozzle diameter, layer height, nozzle temperature, bed temperature, chamber temperature, cooling rate (fan speed), printing speed, and infill percentage [33]. Table 3 lists the manufacturing process and design parameters of the 3D-printed tensile specimens investigated in this study.

Table 3. Manufacturing and design parameters for 3D printing.

Manufacturing/Design parameter	Value	Manufacturing/Design parameter	Value
Build orientation	XYZ	Material	ABS Prime
Filament diameter	1.75 mm	Nozzle diameter	0.4 mm
Layer height	0.2 mm	Nozzle temperature	240 °C
Bed temperature	100 °C	Chamber temperature	90 °C
Cooling	No fan cooling	Raster path	0° (see Section 2.2.1)
Printing speed	2400 mm/min	Infill percentage	100%

The extrudate widths of 0.48 mm and 0.58 mm were used for the perimeters and the infill rasters, respectively. The same ABS spool used for filament tensile testing was used for the 3D printing of seven ASTM D638 Type I specimens. The spool was dehydrated at 60 °C for four hours, and a StatPro ADL-3D77 filament dry cabinet (Production Automation Corporation, Minnetonka, USA) with molecular sieve desiccant packages was used to maintain a dry state. An M2+ 3D printer (AON3D, Montreal, Canada) with a carbon fiber-poly ether ether ketone (CF-PEEK) build platform was used for specimen manufacturing. Simplify3D version 4.1.2 was the slicer for raster path generation. After 3D printing, the specimens were left inside the chamber for eight hours under printing conditions. Then, all heaters were turned off, and the chamber temperature was set to 30 °C activating the chamber fan for uniform cooling. Figure 5 shows the 3D-printed specimens before tensile testing.

Figure 5. 3D-printed ASTM D638 Type I specimens after the MEX additive manufacturing.

2.2.3 Dog-bone specimen testing procedure

Six 3D-printed ABS samples were subjected to a uniaxial tensile loading test using an Instron ElectroPlus E3000 (Instron, Norwood, USA) equipped with a 3 kN load cell. During testing, temperature and humidity ranged between 20 to 24 °C and 22% to 37% RH, respectively. The samples were loaded at a constant crosshead speed of 5 mm/min, according to ASTM D638-22, and the Digital Image Correlation (DIC) gage length was 50 mm. The initial cross-sectional areas of the samples were measured using the same digital micrometer model used for the filament testing. The sample displacement was measured on one side using a 2D DIC system synchronized with the Instron test frame to correlate the strain calculated using the DIC system with the corresponding measured stress from the test frame. For synchronization, an output channel (representing the load) from the analog I/O connection on the rear panel of the Instron controller was connected to the analog-to-digital converter (ADC) in the LaVision system used to control

image acquisition. Therefore, load readings were recorded simultaneously with the images acquired using the LaVision system. More details describing the DIC measurements are provided in Section 2.2.4. The stress-strain curves of the samples were plotted to obtain Young's modulus, stress at yield, stress at break, strain at yield, and strain at break.

2.2.4 DIC strain measurement

The ABS dog-bone tensile specimens were painted with a base coat of flat black spray paint (Rust-Oleum, Concord, ON) on one surface of the sample. A speckling pattern of airbrush paint (Opaque White 5212, Createx Colors, East Granby, CT) was applied over the base coat using an H-Set airbrush (Paasche Airbrush Company, Chicago, IL). A fine stippling effect was achieved by spraying paint onto a flat surface (a wooden tongue depressor) directed at the panel and dispersing small droplets that created a pseudo-random pattern. The samples obtained after speckling are shown in Figure 6.

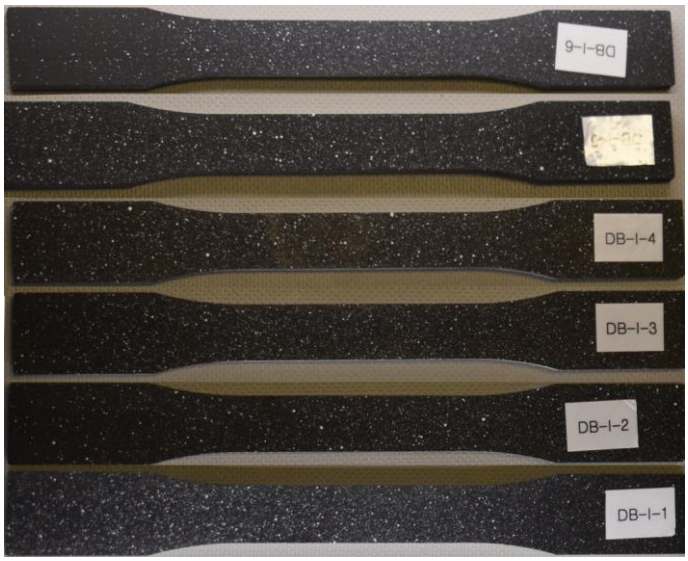

Figure 6. ABS Type I dog-bone tensile testing samples after painting black and speckling on one surface.

The painted surfaces of the dog-bone samples were imaged for DIC during tensile testing using a high-resolution Imager M-Lite 5M camera (LaVision GmbH, Göttingen, Germany) equipped with an MVL50M23 50 mm fixed focal length lens (Navitar, Rochester, NY), acquiring images at five frames per second. Illumination was supplied using two Linear Illumination Units 1103314 (LaVision GmbH, Göttingen, Germany). The camera and image properties are listed in Table 4, and the imaging setup is shown in Figure 7.

Table 4. Camera and image properties for DIC imaging.

Property	Unit	Value
Camera Resolution	px × px	2464 × 2056
Pixel Size	μm	3.45
Frame Rate	Hz	5
Image Scaling Factor	px / mm	17.4
Image Field of View	mm × mm	141.9 × 118.4

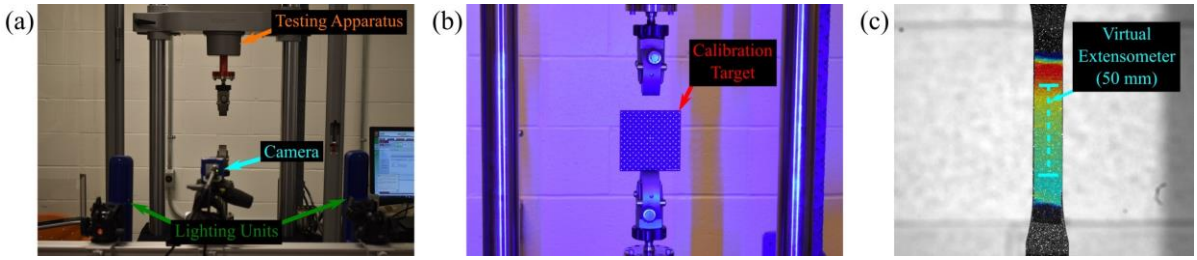

Figure 7. DIC imaging procedure: (a) Imaging setup for tensile testing; (b) Calibration setup; and (c) Representative DIC strain field.

The camera and lighting units are mounted on a tripod along a rail. The calibration target occupied the camera's field of view so that the sample measurements could be reliably converted into real units. Images were processed using the DaVis 10.0.3 commercial DIC software package (LaVision GmbH, Göttingen, Germany), in which 2D deformations and strains were evaluated across the painted surface at each frame, as shown in Figure 7c. Calibration for DIC was performed by acquiring images from a two-level 3D calibration plate Type 106-10 (LaVision GmbH, Göttingen, Germany), as shown in Figure 7b. For each frame before sample failure, the correlation was performed relative to the first frame to prevent compounding precision errors, and a subset size of 25 pixels and a step size of 8 pixels were used to achieve sufficient spatial resolution of the DIC measurements.

3. Results and discussion

This section summarizes the tensile test results for the filament and 3D-printed dog-bone specimens. An outlier detection assessment was performed on the results using the maximum normed residual (MNR) method with a significance level of 0.05 [34].

3.1 Filament testing results

Nine sets of tests, each with at least eight samples, were completed, as listed in Table 2 (a total of 76). The following tensile properties were obtained: Young's modulus, stress at yield, stress at break, strain at yield, strain at break, and maximum crosshead movement. Note that experiment A did not include an extensometer; therefore, strain-based parameters were not evaluated. Furthermore, necking of the filaments was observed during the tests, particularly outside the

extensometer gage region. The data repository for this study included output files from the testing machine, analyzed results, two video recordings, and all notes regarding the observed necking. For the modulus calculations, portions of the stress-strain curve between 5.00 and 35.0 MPa were considered, which corresponded to 10% and 80% of the stress at yield, respectively. If the exact stress range endpoints were unavailable, the closest available data points were used. Extensometer slippage occurred during the testing of 18 specimens, and the total slippage was calculated to determine the correct strain at the yield and break values.

Table 5 lists the filament tensile test results for experiments A (no extensometer), B (extensometer with blunt knife edges), and C (extensometer with standard knife edges). Because set A did not include an extensometer, Young's modulus and strain values were not calculated. Sets B and C measured similar Young's moduli with low coefficients of variation (CV). Therefore, both blunt and standard knife-edge types can accurately measure this property. The CV is the standard deviation of the test set over the test set mean and is expressed as a percentage. Typically, a CV of less than 10% is considered good, and a CV of less than 5% is considered very good.

Although the crosshead movement, particularly at low strain values, is generally not recommended for accurate modulus calculations, some researchers have used it in the past. For example, if the crosshead movement and the resulting elongation percentage were used for the modulus calculation for set A, an average value of 0.600 GPa was obtained. This average value is very much in error compared to the extensometer-based calculations for sets B and C. Therefore, it can be concluded that crosshead movement cannot be used for modulus determination and an extensometer is required.

Table 5. Filament tensile test results for sets A, B, and C.

Experiment ID	Young's modulus		Stress at yield		Stress at break		Strain at yield		Strain at break		Crosshead movement	
	AVG (GPa)	CV (%)	AVG (MPa)	CV (%)	AVG (MPa)	CV (%)	AVG (%)	CV (%)	AVG (%)	CV (%)	AVG (mm)	CV (%)
A	N/A	N/A	43.4	1.6	39.3	4.4	N/A	N/A	N/A	N/A	32.8	63
B	2.20	3.8	43.9	1.2	39.1	4.1	2.69	8.6	23.0	59	37.8	67
C	2.29	1.5	44.3	1.5	42.4	2.3	2.66*	2.5*	4.85	35	15.4	13

* Sample C-2 was detected as an outlier for the strain at yield and was removed from the calculations.

The stresses at yield for all sets were similar, with low CV; therefore, an extensometer with blunt or standard knife edges could measure this property accurately. Although the average crosshead movements for sets A and B were similar, set C had a significantly lower value. This indicates that the extensometer with a standard knife edge resulted in the premature failure of the filaments, with a breakage point at the lower knife edge. A large variation was observed in the crosshead movement results for both experiments A and B. During testing, some samples did not show necking and failed at a much lower crosshead movement than those with multiple necking locations. Figure 8a shows the significant necking observed for sample B-7. It is hypothesized that

defects may be distributed randomly along the filaments, and if they are present in the test gage length, they can cause failure at lower crosshead movements without necking. For the extensometer with a standard knife edge, the impact of the knife edge is considered greater than the potential defects, resulting in no necking in the samples and lower levels of crosshead movement leading to failure. Figure 8b shows sample C-3 before failure with no necking.

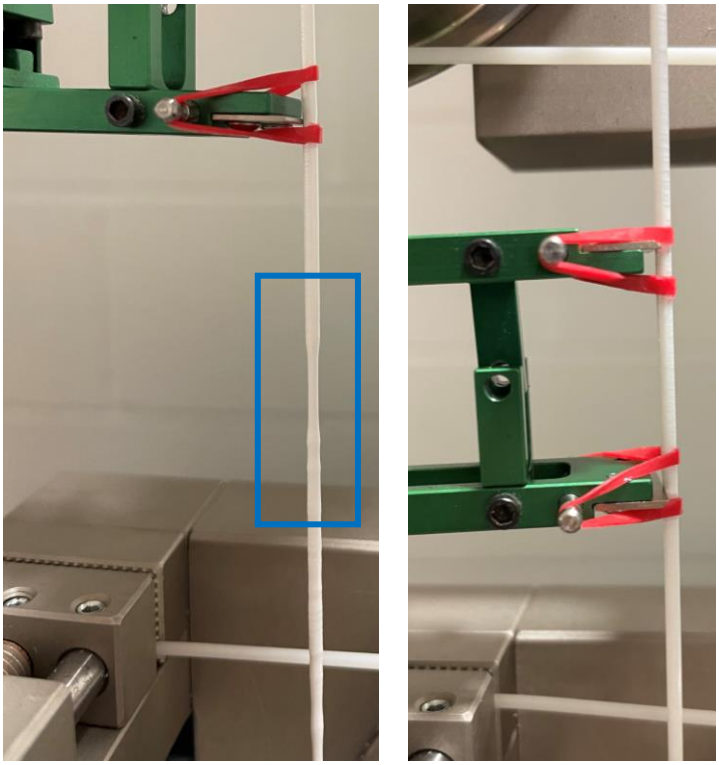

(a) **(b)**

Figure 8. Filaments during tensile testing: (a) extensive necking outside extensometer gage for specimen B-7; and (b) no necking for specimen C-3.

The minimum, maximum, and median crosshead movements in experiments A (13.9, 66.8, and 23.3 mm) and B (12.9, 96.8, and 29.5 mm) were similar. Hence, an extensometer with a blunt knife edge can be successfully used for strain measurements without creating stress concentrations or premature failure in the filaments. Necking in the samples results in a smaller cross-sectional area at the location of failure; however, because only engineering stresses are considered in this study, they will have lower stresses at the break. This can be observed in Table 5, where the stresses at the break for sets A and B are similar and lower than 42.4 MPa for set C. There was no necking in the filaments before yield; therefore, the extensometer could measure strain values accurately up to this point, as is evident from the strain at yield values for sets B and C, which were similar. However, after yield and necking in the filaments, especially for set B, the extensometer could not be used for strain measurement because necking mainly occurred outside the extensometer gage section. Therefore, the table shows a high CV for the strain at break for set B, with a lower

variability for set C. Although the extensometer could not provide an accurate measure of the strain at break, set B failed at much higher strain values than set C.

As listed in Table 5, for sets A, B, and C, Young's modulus, stress at yield, and strain at yield were similar. It is considered that normal sample variability caused the observed variations. Outlier detection was performed on Young's modulus, stress at yield, and strain at yield, and only the strain at yield value for sample C-2 was detected as an outlier. This information has been removed from the statistical analyses listed in Table 5. Because the hypothesized random distribution of defects would only seriously impact the stress at break, strain at break, and crosshead movement, the authors did not perform outlier detection on these properties.

From experiments A, B, and C, it was concluded that an extensometer with blunt knife edges could be effectively used to evaluate filament tensile properties. Therefore, set B was selected as the baseline. Note that its tensile modulus and strength of 2.20 GPa and 39.1 GPa, respectively, are in line with the reported values for neat ABS by Ansari et al. (2.3 GPa and 39.3 MPa) [17]. Table 6 lists the results for a gage length of 250 mm (experiment D) and compares the values with the set B, which has a gage length of 165 mm. The crosshead movement for set D was over a longer gage length compared to set B; therefore, the total crosshead movement was reduced proportionally to correspond to the same gage length as in set B for comparison purposes. No outliers were detected for Young's modulus, stress at yield, and strain at yield.

Table 6. Filament tensile test results for sets B and D.

Experiment ID	Young's modulus		Stress at yield		Stress at break		Strain at yield		Strain at break		Crosshead movement	
	AVG (GPa)	CV (%)	AVG (MPa)	CV (%)	AVG (MPa)	CV (%)	AVG (%)	CV (%)	AVG (%)	CV (%)	AVG (mm)	CV (%)
B	2.20	3.8	43.9	1.2	39.1	4.1	2.69	8.6	23.0	59	37.8	67
D	2.26	2.2	44.3	1.2	40.8	3.7	2.54	8.5	12.0	69	21.3*	41

* Crosshead movement is reduced proportionally for comparison.

Table 6 shows there was low variability in all tensile properties up to yield, and there were large CVs for strain at break and crosshead movement. For set D, necking outside the extensometer gage was observed for all samples. Figure 9 shows necking in specimens D-1 and D-6 before failure, which is less extensive than the necking observed for specimen B-7 (Figure 8a).

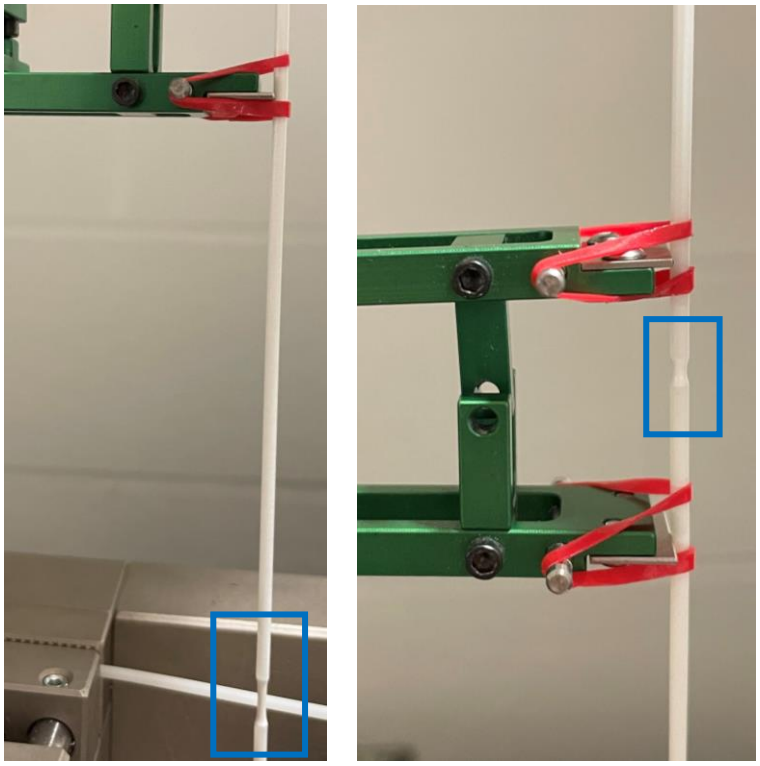

(a) **(b)**

Figure 9. Filaments during tensile testing: (a) some necking for D-1 outside extensometer gage; and (b) small necking for D-6 within extensometer gage.

Compared with the baseline (experiment B), the longer gage length in experiment D provided no significant changes in the measured Young's modulus, stress at break, stress at yield, or strain at yield but did cause a significant reduction in the total crosshead movement. It can be concluded that a longer gage length may affect the total displacement until failure. Therefore, experiment B is kept as the baseline.

Experiments E, F, G, and H explored the impact of the testing speed on the filament tensile properties at speeds of half, two, four, and ten times the baseline, respectively (3.30, 12.7, 25.4, and 63.5 mm/min (0.13, 0.5, 1.0, and 2.5 in./min)). Table 7 lists the results and compares them to those of the baseline (set B). Note that for one sample in set F (F-4) and two samples in set G (G-1 and G-4), the extensometer limit was reached before filament failure. For these specimens, failure was considered the point of maximum recorded strain. No outliers were detected for Young's modulus, stress at yield, or strain at yield.

Table 7. Filament tensile test results for sets E, B, F, G, and H.

Experiment ID	Young's modulus		Stress at yield		Stress at break		Strain at yield		Strain at break		Crosshead movement	
	AVG (GPa)	CV (%)	AVG (MPa)	CV (%)	AVG (MPa)	CV (%)	AVG (%)	CV (%)	AVG (%)	CV (%)	AVG (mm)	CV (%)
E	2.20	3.1	43.0	0.71	38.5	2.2	2.84	10	20.2	57	45.0	43
B	2.20	3.8	43.9	1.2	39.1	4.1	2.69	8.6	23.0	59	37.8	67
F	2.31	4.1	45.2	1.5	39.7	1.4	2.62	8.5	19.7[1]	87	36.4	59
G	2.32	2.4	46.5	1.2	41.0	4.8	2.83	6.9	26.0[2]	77	32.6	51
H	2.36	2.4	48.2	1.6	41.7	4.8	2.77	6.0	11.4	38	22.5	25

[1] For one sample in set F, the extensometer limit was reached before filament failure.

[2] For two samples in set G, the extensometer limit was reached before filament failure.

Generally, with an increase in testing speed from set E to sets B, F, G, and H, Table 7 shows that there were modest increases in Young's modulus, stress at yield, and stress at break. The increases over this range were more significant for the stress at yield (an increase of 12%) than for the stress at break (an increase of 8.4%) and Young's modulus (an increase of 7.2%). There was also a reduction in the average crosshead movement with increasing test speed, although the high variability in this measurement made it difficult to draw conclusions. Neither the strain at yield nor the strain at break showed a clear relationship with the testing speed.

More necking near the top or bottom bollard was observed for set E than for set B. Figure 10a shows that sample E-8 exhibited significant necking near the top bollard. Figure 10b shows sample F-4 with necking outside the extensometer gage length, similar to that previously observed for other sets, e.g., set B. Sample G-4 with significant necking within the extensometer gage length is shown in Figure 10c. The test for sample G-4 was stopped at a strain of 47.7%, considering the extensometer displacement limit. The crosshead movement of sample G-4 was smaller than that of sample F-4, whereas a larger strain at break was recorded by the extensometer for sample G-4. This indicates that the strain values from the extensometer cannot be relied upon when significant necking occurs outside the gage length.

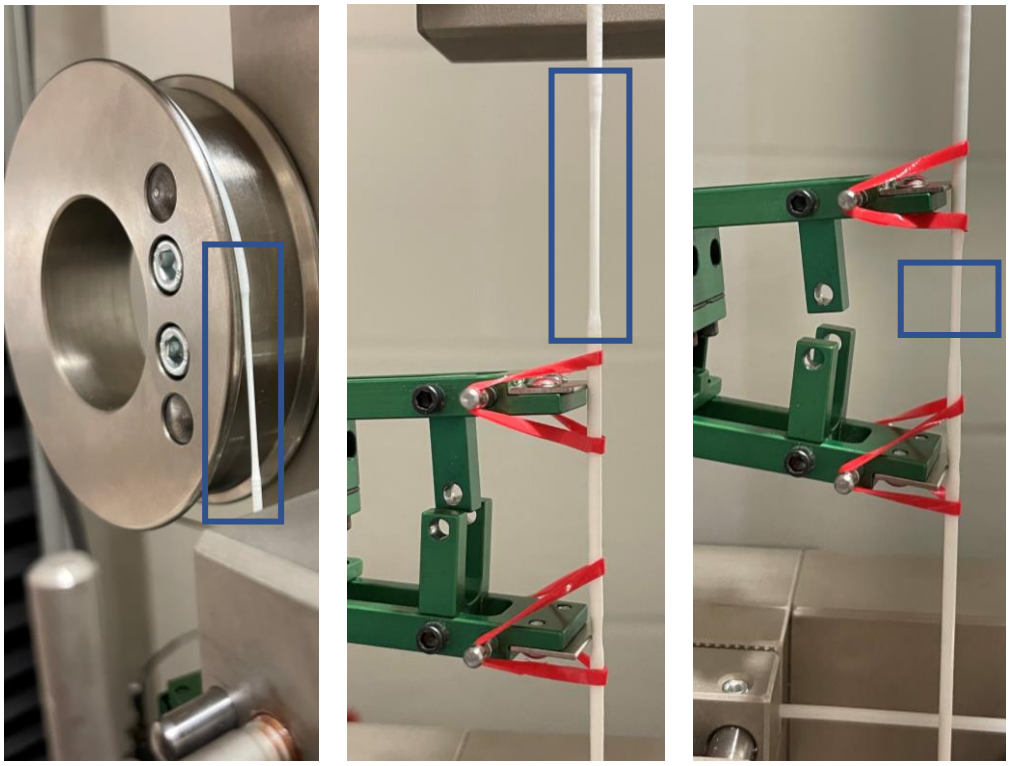

(a) **(b)** **(c)**

Figure 10. Filaments during tensile testing: (a) significant necking at the top bollard for sample E-8; (b) significant necking above the extensometer for sample F-4; and (c) significant necking in the extensometer gage length for sample G-4.

Sets E and B had very similar tensile properties; therefore, the test parameters for set B, with a higher testing speed and demonstrated failure locations closer to the middle of the filament gage length, were recommended as the baseline.

The final set of tests (experiment I) explored the impact of the oven treatment on the tensile properties of the filaments. As mentioned in Section 2.1.2, after the oven treatment, the filament slumped on the spool and was wavy. It was challenging to straighten the filament using preloading, which created irregularities in the stress-strain curve. Therefore, only the stresses at yield and break are listed in Table 8. The data repository for this study includes figures for the oven-treated samples after cutting and placement in the fixture. No outliers were detected for stress at yield.

Table 8. Filament tensile test results for sets B and I.

Experiment ID	Young's modulus		Stress at yield		Stress at break		Strain at yield		Strain at break		Crosshead movement	
	AVG (GPa)	CV (%)	AVG (MPa)	CV (%)	AVG (MPa)	CV (%)	AVG (%)	CV (%)	AVG (%)	CV (%)	AVG (mm)	CV (%)
B	2.20	3.8	43.9	1.2	39.1	4.1	2.69	8.6	23.0	59	37.8	67
I	N/A	N/A	39.8	0.92	38.4	2.6	N/A	N/A	N/A	N/A	N/A	N/A

There was a modest reduction of 9.2% in stress at yield after oven treatment, which agrees with a 12.5% reduction in strength observed in a previous study conducted by the authors [22]. In addition, the stress at break was reduced to a lesser extent (1.8%), suggesting that the oven treatment had only a small effect on the material properties. In future studies, oven treatment of individually cut filaments will be conducted to prevent the waviness of the samples caused by post-processing and to explore the impact of oven treatment on other tensile properties.

The failure locations of all the filament samples were recorded. Table 9 lists the averages and CVs of the failure locations as percentages of the final filament gage length. This was determined from the post-test length of the filament bottom piece measured from the bottom of the gage section (Figure 3). 50% indicates that the failure occurred exactly in the middle of the final gage length (after maximum crosshead movement). Failure locations at the bottom and top bollards are indicated by 0% and 100%, respectively.

Table 9. Failure location for all filament tensile tests.

Experiment ID	AVG (%)	CV (%)	Experiment ID	AVG (%)	CV (%)
A	58	44	F	59	25
B	44	34	G	53	36
C	41	1.6	H	43	16
D	54	51	I	36	55
E	48	85			

For many sets, the average of the failure locations is observed to be close to the middle of the filament final test section length, and the CVs are quite high, with one exception. If, as hypothesized, defects that control failure location are distributed randomly along the filament length, this would result in variability in the failure location and an average close to the gage length midpoint, which agrees with most datasets listed in Table 9. For set C (extensometer with standard knife edges), there was a very low CV (only 1.6%), and the failure location was close to the lower knife edge location. The lower knife edge is believed to have a greater effect than the upper knife edge because of the weight of the extensometer pressing it into the filament (Figure 3). This indicates that standard knife edges had a higher impact on breakage than defects and may have resulted in premature failure. This agrees with the findings of the strain at break and crosshead movement for set C listed in Table 5.

3.2 Testing results for dog-bone specimens

Figure 11 shows the 3D-printed dog-bone specimens obtained after testing. The machine crosshead movement limit was reached for four samples, and they did not break. For the two ruptured samples (DB-I-1 and DB-I-6), a crack was initiated in the narrow cross-sectional test section and propagated until it reached the middle of the specimen, indicating an acceptable failure mode

according to ASTM D638. At this point, the crack changed direction and moved along both the specimen length and around the infill in the grip sections. The slicer limitations in adjusting the width of a single linear extrusion in the optimized raster path (Figure 4) may have resulted in voids along the specimen length, which will be explored in a future study. In addition, a testing machine with a higher crosshead movement limit is required.

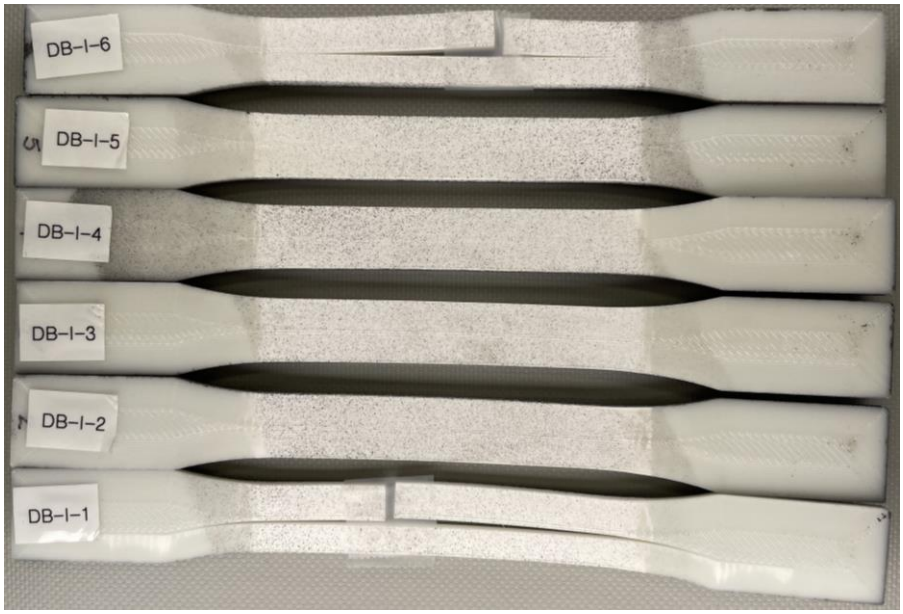

Figure 11. 3D-printed ASTM D638 Type I specimens after tensile testing (non-painted side).

Figure 12 shows the stress-strain curves obtained from tensile testing of the 3D-printed specimens. The ABS samples behaved in a ductile manner, as indicated by the plateau curve after the yield point, which has also been reported in the literature [35, 36]. Because specimens DB-I-2, -3, -4, and -5 did not fail and exceeded the extension limit of the test frame, their stress-strain graphs returned to zero. For these specimens, failure was considered as the point of maximum recorded strain.

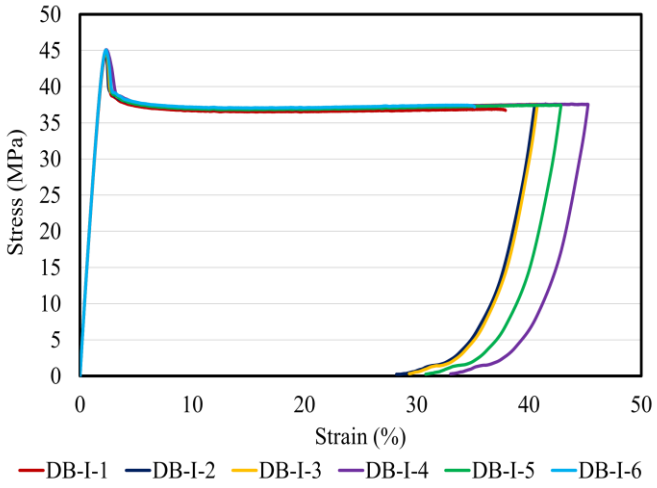

Figure 12. Stress-strain curves of 3D-printed Type I dog-bone ABS samples.

Table 10 lists the following tensile properties of the 3D-printed specimens: Young's modulus, stress at yield, stress at break, strain at yield, and strain at break. Similar to the filament tensile properties, a portion of the stress-strain curves between 5.00 and 35.0 MPa was used for the modulus calculations. The MNR method was used, and no outliers were detected in the tensile properties of the dog-bone specimens. Previous studies reported a large variability in dog-bone tensile results when a 0º raster angle was used [23]. Table 10 shows that the CVs for all the tensile results, except the strain at break and crosshead movement, were very low (less than 1.5%). In addition, the strain at break and total crosshead movement provided reasonable CV values, which demonstrated the effectiveness of the optimized raster path used to 3D-print the specimens.

Table 10. Tensile properties of 3D-printed Type I dog-bone ABS samples.

Specimen ID	Young's Modulus (GPa)	Stress at yield (MPa)	Stress at break (MPa)	Strain at yield (%)	Strain at break (%)	Crosshead movement (mm)
DB-I-1	2.24	44.5	36.7	2.27	37.9	26.9
DB-I-2	2.27	44.7	37.4	2.25	40.5*	28.0*
DB-I-3	2.27	44.9	37.5	2.28	40.7*	28.0*
DB-I-4	2.26	45.1	37.5	2.35	45.3*	29.0*
DB-I-5	2.26	44.9	37.4	2.31	42.8*	29.0*
DB-I-6	2.27	45.1	37.2	2.31	35.2	24.8
Average	2.26	44.9	37.3	2.30	40.4*	27.6*
CV (%)	0.53	0.51	0.80	1.5	8.8*	5.8*

* The crosshead movement limit was reached before failure.

Table 11 lists the tensile results for the optimum filament test set (B) and compares them with the results for the 3D-printed dog-bone tensile specimens. For the 3D-printed dog-bone specimens, the total crosshead movement increased proportionally, considering their shorter grip-to-grip distance of 115 mm compared to set B with a filament gage length of 165 mm.

Table 11. Tensile test results for filaments and 3D-printed dog-bone specimens.

Experiment ID	Young's modulus		Stress at yield		Stress at break		Strain at yield		Strain at break		Crosshead movement	
	AVG (GPa)	CV (%)	AVG (MPa)	CV (%)	AVG (MPa)	CV (%)	AVG (%)	CV (%)	AVG (%)	CV (%)	AVG (mm)	CV (%)
Set B (Filament)	2.20	3.8	43.9	1.2	39.1	4.1	2.69	8.6	22.3	55	37.8	67
Dog-bone	2.26	0.53	44.9	0.51	37.3	0.80	2.30	1.5	40.4	8.8	39.6*	5.8

* The crosshead movement was increased proportionally for comparison purposes.

The filament and 3D-printed dog-bone tensile tests provided very similar results for Young's modulus, stress at yield, stress at break, and crosshead movement. The 3D-printed samples exhibited a slightly lower strain at yield, which was reduced by 14.6% compared to the filament

average. Significant necking occurred outside the extensometer gage length during the filament tests. Therefore, no conclusion could be drawn from the strain-at-break values.

As explained in Section 1, 3D-printed dog-bone specimens in the literature mainly exhibit breakage in the transition area and consequently provide lower tensile properties than filament tests. However, the raster path in this study was successfully optimized, resulting in specimen breakage within a narrow cross-sectional test section (an acceptable failure mode). This proves that dog-bone tensile specimens with 0° rasters can be 3D-printed with minimal defects. Therefore, it is not necessary to modify the dimensions of the dog-bone specimens to achieve an acceptable failure mode for 0° rasters, and the ASTM D638 Type I specimen, the preferred specimen, can be used in the field of the MEX process.

In this study, dog-bone tensile properties are shown to be similar to filament-derived "bulk material" properties. Therefore, the 3D-printed dog-bone tensile results confirm the filament tensile results. They showed that the tensile properties of ABS could be accurately evaluated using a set of bollard-type test fixtures and the filament testing parameters of set B, that is, an extensometer with blunt knife edges, a gage length of 165 mm, and a testing speed of 6.35 mm/min (0.25 in./min). Note that different polymers and reinforcement types may require a re-evaluation of these testing parameters.

4. Conclusions

This study provides comprehensive experimental data on filament tensile testing to help develop an optimized test method for measuring filament tensile properties. It explored the impact of the strain measurement device, extensometer knife-edge type, filament gage length, testing speed, and oven treatment on the tensile properties of an acrylonitrile butadiene styrene (ABS) filament using an off-the-shelf bollard-type fixture.

It was observed that an extensometer with a standard knife-edge accurately evaluated the filament tensile properties up to yield; however, it caused premature failure in the filament after yielding. It was determined that an extensometer with blunt knife edges introduced minimal disturbance to the specimens while still providing accurate elongation measurements. With an increase in the testing speed, there were modest increases in the stress at yield, stress at break, and Young's modulus. The oven-treatment process resulted in a modest reduction in stress at yield, whereas the reduction in stress at break was not significant.

Therefore, it was concluded that using an off-the-shelf bollard-type fixture, an extensometer with blunt knife edges, a gage length of 165 mm, and 6.35 mm/min (0.25 in./min) testing speed can accurately evaluate the tensile properties of ABS filaments.

The tensile properties of the 3D-printed dog-bone specimens exhibited very low CV values, validating the effectiveness of the optimized raster path. Their Young's modulus, stress at yield, and stress at break (2.26 GPa, 44.9 MPa, and 37.3 MPa) were very similar to those of the baseline filament test (2.20 GPa, 43.9 MPa, and 39.1 MPa). This provides further confidence in the filament tensile results and demonstrates the effectiveness of the optimized raster path.

The optimized filament tensile test reported here can reliably provide baseline values that can serve as a foundation for AM process development. Furthermore, filament tensile testing can be used to evaluate feedstock properties without using 3D-printed dog-bone specimens. In this study, filament tensile testing was explored for one polymeric material without reinforcement. High-performance polymers such as ULTEM^{TM} 9085 and Victrex AM^{TM} 200 and reinforced filaments will be explored in future studies. All information from this study, such as the oven-treatment process, raw output files from testing machines, analyzed results, and factory files for 3D printing, is provided in the data repository so that other researchers can use it for future filament tensile studies.

Statements & Declarations

CRediT authorship contribution statement

Santiago Rodrigues: Formal analysis, Investigation, Data Curation, Writing - Original Draft; **Seyed Miri**: Methodology, Investigation, Resources; **Richard G. Cole:** Methodology, Writing - Original Draft, Writing - Review & Editing, Resources, Funding acquisition; **Abraham Avalos Postigo**: Methodology, Writing - Original Draft, Writing - Review & Editing, Resources, Funding acquisition; **Menna A Saleh:** Formal analysis, Investigation, Data Curation, Writing - Original Draft; **Alexander Dondish:** Formal analysis, Investigation, Data Curation, Writing - Original Draft; **Garrett W. Melenka:** Formal analysis, Investigation, Data Curation, Writing - Original Draft, Project Administration, Supervision; **Kazem Fayazbakhsh:** Conceptualization, Methodology, Investigation, Resources, Writing - Original Draft, Writing - Review & Editing, Supervision, Project administration, Funding acquisition.

Data availability statement

All information from this study, e.g., oven-treatment process, raw output files from testing machines, and analyzed results, is provided in the data repository (Mendeley Data, V1: https://doi.org/10.17632/4h2v2yctf4.1).

Declaration of competing interest

The authors declare that they have no known competing financial interests or personal relationships that could have appeared to influence the work reported in this paper.

Acknowledgment

The authors would like to thank Dr. Ghaemi for all his supports during the tensile testing campaign. Financial support from the Natural Sciences and Engineering Research Council of Canada (NSERC), RGPIN-2018-04144, the National Research Council Canada (NRC), and Toronto Metropolitan University-Undergraduate Research (URO) are appreciated.

References

[1] Spörk, M., Savandaiah, C., Arbeiter, F., Schuschnigg, S. and Holzer, C., 2017. Properties of glass filled polypropylene for fused filament fabrication. Proceedings of the ANTEC Anaheim, pp.105-111.

[2] Spoerk, Martin, Florian Arbeiter, Ivan Raguž, Georg Weingrill, Thomas Fischinger, Gerhard Traxler, Stephan Schuschnigg, Ludwig Cardon, and Clemens Holzer. "Polypropylene filled with glass spheres in extrusion-based additive manufacturing: effect of filler size and printing chamber temperature." Macromolecular Materials and Engineering 303, no. 7 (2018): 1800179.

[3] M. Milosevic, D. Stoof, and K. Pickering, "Characterizing the mechanical properties of fused deposition modelling natural fiber recycled polypropylene composites," Journal of Composites Science, vol. 1, no. 1, 7, Jul. 2017, doi: 10.3390/jcs1010007

[4] Kaynak, B., Spoerk, M., Shirole, A., Ziegler, W. and Sapkota, J., 2018. Polypropylene/cellulose composites for material extrusion additive manufacturing. Macromolecular Materials and Engineering, 303(5), p.1800037.

[5] Guessasma, S., Belhabib, S. and Nouri, H., 2019. Microstructure and mechanical performance of 3D printed wood-PLA/PHA using fused deposition modelling: Effect of printing temperature. Polymers, 11(11), p.1778.

[6] Guessasma, S., Belhabib, S. and Altin, A., 2020. On the tensile behaviour of bio-sourced 3D-printed structures from a microstructural perspective. Polymers, 12(5), p.1060.

[7] Santo, J., Penumakala, P.K. and Adusumalli, R.B., 2021. Mechanical and electrical properties of three-dimensional printed polylactic acid–graphene–ca rbon nanofiber composites. Polymer Composites, 42(7), pp.3231-3242.

[8] Lohar, D.V., Nikalje, A.M. and Damle, P.G., 2022. Development and testing of hybrid green polymer composite (HGPC) filaments of PLA reinforced with waste bio fillers. Materials Today: Proceedings.

[9] Bharath, H.S., Bonthu, D., Prabhakar, P. and Doddamani, M., 2020. Three-dimensional printed lightweight composite foams. ACS omega, 5(35), p.22536.

[10] Delgado, G.F., Pinho, A.C. and Piedade, A.P., 2022. 3D Printing for Cartilage Replacement: A Preliminary Study to Explore New Polymers. Polymers 2022, 14, 1044.

[11] K. Abouzaid, S. Guessasma, S. Belhabib, D. Bassir, and A. Chouaf, "Thermal mechanical characterization of Copolyester for additive manufacturing using FDM," International Journal for Simulation and Multidisciplinary Design Optimization, vol. 10, A9, Jun. 2019, doi: 10.1051/smdo/2019011

[12] Hachimi, T., Naboulsi, N., Majid, F., Rhanim, R., Mrani, I. and Rhanim, H., 2021. Design and Manufacturing of a 3D printer filaments extruder. Procedia Structural Integrity, 33, pp.907-916.

[13] Vidakis, N., Petousis, M., Grammatikos, S., Papadakis, V., Korlos, A. and Mountakis, N., 2022. High Performance Polycarbonate Nanocomposites Mechanically Boosted with Titanium Carbide in Material Extrusion Additive Manufacturing. Nanomaterials, 12(7), p.1068.

[14] Syaifuddin, M., Suryanto, H. and Suprayitno, S., 2021. The Effect of Multi-Extrusion Process of Polylactic Acid on Tensile Strength and Fracture Morphology of Filament Product. Journal of Mechanical Engineering Science and Technology (JMEST), 5(1), pp.62-72.

[15] Uddin, M., Williams, D. and Blencowe, A., 2021. Recycling of Selective Laser Sintering Waste Nylon Powders into Fused Filament Fabrication Parts Reinforced with Mg Particles. Polymers, 13(13), p.2046.
[16] Fang, L., 2020. Characterization and optimization of geometrical accuracy and mechanical properties of specimens prepared by fused filament fabrication, Ph.D. dissertation, Whiting School of Engineering, Johns Hopkins University, Baltimore, U.S, 2020
[17] Ansari, M.Q., Redmann, A., Osswald, T.A., Bortner, M.J. and Baird, D.G., 2019. Application of thermotropic liquid crystalline polymer reinforced acrylonitrile butadiene styrene in fused filament fabrication. Additive Manufacturing, 29, p.100813.
[18] Bi, X., Tan, H., Li, Z., Li, Y. and Liu, T., 2020, February. Research on Preparation Technology for Continuous Carbon Fiber Reinforced Printing Filaments. In IOP Conference Series: Materials Science and Engineering (Vol. 772, No. 1, p. 012084). IOP Publishing.
[19] Nazemzadeh, Nogol, Anahita Ahmadi Soufivand, and Nabiollah Abolfathi. "Computing the bond strength of 3D printed polylactic acid scaffolds in mode I and II using experimental tests, finite element method and cohesive zone modeling." The International Journal of Advanced Manufacturing Technology 118, no. 7 (2022): 2651-2667.
[20] Rahimizadeh, A., Kalman, J., Fayazbakhsh, K. and Lessard, L., 2019. Recycling of fiberglass wind turbine blades into reinforced filaments for use in Additive Manufacturing. Composites Part B: Engineering, 175, p.107101.
[21] Ferreira, Isaac, Diogo Vale, Margarida Machado, and Jorge Lino. "Additive manufacturing of polyethylene terephthalate glycol/carbon fiber composites: An experimental study from filament to printed parts." Proceedings of the Institution of Mechanical Engineers, Part L: Journal of Materials: Design and Applications 233, no. 9 (2019): 1866-1878.
[22] R. G. Cole, K. Fayazbakhsh, A. Avalos, and N. A. Nadeau, “Improved test methods for polymer additive manufacturing interlayer weld strength and filament mechanical properties,” Progress in additive manufacturing 2020, ASTM STP 1637, pp. 325–338, Feb. 2022, doi: 10.1520/stp163720200107
[23] Yıldız, A., Emanetoğlu, U., Yenigun, E.O. and Cebeci, H., 2022. Towards optimized carbon nanotubes (CNTs) reinforced polyetherimide (PEI) 3D printed structures: A comparative study on testing standards. Composite Structures, p.115853.
[24] Sola, A., Chong, W.J., Simunec, D.P., Li, Y., Trinchi, A., Kyratzis, I.L. and Wen, C., 2023. Open challenges in tensile testing of additively manufactured polymers: A literature survey and a case study in fused filament fabrication. Polymer Testing, p.107859.
[25] Mark-10 company https://mark-10.com/products/grips-attachments/wire-rope-yarn-tubing/wire-rope-grip-bollard-style-high-capacity-g1092/#tab-0 (accessed 17 Nov. 2022).
[26] J. Rodriguez, J. Thomas, and J. Renaud, “Mechanical Behavior of Acrylonitrile Butadiene Styrene (ABS) Fused Deposition Materials—Experimental Investigation,” Rapid Prototyping Journal 7, no. 3 (2001): 148–158, https://doi.org/10.1108/13552540110395547
[27] Epsilon Technology, https://www.epsilontech.com/products/extensometer-knife-edges/ (accessed 14 Dec. 2022).
[28] Auffray, L., Gouge, P.A. and Hattali, L., 2022. Design of experiment analysis on tensile properties of PLA samples produced by fused filament fabrication. The International Journal of Advanced Manufacturing Technology, pp.1-15.
[29] Özen, A., Auhl, D., Völlmecke, C., Kiendl, J. and Abali, B.E., 2021. Optimization of manufacturing parameters and tensile specimen geometry for fused deposition modeling (FDM) 3D-printed PETG. Materials, 14(10), p.2556.

[30] Uşun, A. and Gümrük, R., 2021. The mechanical performance of the 3D printed composites produced with continuous carbon fiber reinforced filaments obtained via melt impregnation. Additive Manufacturing, 46, p.102112.
[31] Ferrell, W.H., Clement, J. and TerMaath, S., 2021. Uniaxial tensile testing standardization for the qualification of fiber reinforced plastics for fused filament fabrication. Mechanics of Advanced Materials and Structures, 28(12), pp.1254-1273.
[32] García-Domínguez, Amabel, Juan Claver, Ana María Camacho, and Miguel A. Sebastián. 2020. "Considerations on the Applicability of Test Methods for Mechanical Characterization of Materials Manufactured by FDM" Materials 13, no. 1: 28. https://doi.org/10.3390/ma13010028
[33] Fayazbakhsh, K., Movahedi, M. and Kalman, J., 2019. The impact of defects on tensile properties of 3D printed parts manufactured by fused filament fabrication. Materials Today Communications, 18, pp.140-148.
[34] MIL-HDBK-17F (2002) Composite material handbook, Polymer matrix composite guidelines, vol. 1
[35] Cantrell, J.T., Rohde, S., Damiani, D., Gurnani, R., DiSandro, L., Anton, J., Young, A., Jerez, A., Steinbach, D., Kroese, C. and Ifju, P.G., 2017. Experimental characterization of the mechanical properties of 3D-printed ABS and polycarbonate parts. Rapid Prototyping Journal, 23(4), p.811–824.
[36] Galeja, M., Hejna, A., Kosmela, P. and Kulawik, A., 2020. Static and dynamic mechanical properties of 3D printed ABS as a function of raster angle. Materials, 13(2), p.297. https://doi.org/10.3390/ma13020297.